

Article

Estimation of Effective Diffusion Coefficient of O₂ in Ash Layer in Underground Coal Gasification by Thermogravimetric Apparatus

Xi Lin, Qingya Liu and Zhenyu Liu *

Beijing Advanced Innovation Center for Soft Matter Science and Engineering, and State Key Laboratory of Chemical Resource Engineering, Beijing University of Chemical Technology, Beijing 100029, China; buctlinxi@outlook.com (X.L.); qyliu@mail.buct.edu.cn (Q.L.)

* Correspondence: liuzy@mail.buct.edu.cn; Tel.: +86-(0)10-6442-1073

Received: 28 January 2018; Accepted: 14 February 2018; Published: 22 February 2018

Abstract: Underground coal gasification (UCG) proceeds generally in the presence of an ash layer on coal (or char) surface. The ash layer increases the mass transfer resistance of O₂ to the gasification surface, which may become the limiting step of whole process. This paper studies O₂ diffusion in ash layer formed on cylindrical char samples using a specially designed one-dimension setup in a thermogravimetric apparatus (TGA). The effective internal diffusion coefficient (D_e) is found to increase with an increase in ash layer thickness, due to an increase in median pore diameter. Methods are established to correlate D_e with operating conditions and to estimate the role of internal diffusion resistance in overall mass transfer resistance.

Keywords: underground coal gasification; ash layer; effective diffusion coefficient; internal diffusion resistance

1. Introduction

Underground coal gasification (UCG) has been viewed as a potential technology because it requires no mining and transportation of coal and leaves the gasification residue underground. In UCG, gasification agents, such as O₂ and H₂O, are injected into predrilled cavity in which the reaction of O₂ with coal yields a high temperature, in a range of 1173–1473 K [1], to allow the reactions of H₂O and CO₂ with coal to occur to produce CO and H₂. The CO and H₂ can be used as feedstock for many chemical industries and fuels for various purposes [2]. This process has been tested for more than one hundred years, such as in the former Soviet Union, and has been studied extensively in recent decades in many countries including Poland, China, Australia and Ukraine [3]. These studies, ranged from field scale to laboratory scale, have advanced this technology significantly. However, there is still no commercial application of this technology to date due mainly to difficulties in steady state operation for a sufficient long period of time. Therefore, laboratory studies in all aspects of the process were emphasized by many researchers. For instance, Urych studied UGC in a TGA/DSC system and evaluated pyrolysis of coal, a step prior to gasification, in a temperature range of 298–1173 K [4]. Prabu et al. studied UCG through combustion of wood block and coal in laboratory to simulate the cavity formation [5]. The impact of reactant gas composition and injection rate on UCG product distribution are also studied by laboratory research [6,7].

It has been found in past studies that the main gasification reaction in UCG is the reaction of coal pyrolysis char with the gasification agents, which is also the limiting step in overall UCG process [8]. In this gasification reaction, minerals in char, which usually accounts 10–20 wt. % of coal, up to 50 wt. % in some coals [9], form an ash layer on the char surface due to exhaustion of carbon by

gasification. This ash layer increases the internal resistance of gas and makes the mass transfer of gasification agents the rate controlling step [10,11].

Experimental and numerical modeling studies have been carried out to study mass transfer in the ash layer in UCG. Some experimental studies [12,13] observed formation of cracks and fractures in coal during gasification, which shatters coal char and ash layer and reduces the mass transfer resistance of gasification agents in ash layer. However, this shattering effect was found by a percolation model [14] to be insufficient to diminish the mass transfer limitation of the gasification agents because the new char surface formed would be quickly covered by an ash layer. The laboratory [15] and field test [16] studies of UCG showed that the ash layers in the order of centimeter on the char surface, as well as in char cracks, constitute the major scenes of internal diffusion.

Conventional modeling studies on UCG [17–19] also studied mass transfer of gasification agents from the bulk gas flow to the surface of solid, which depends largely on temperature distribution and turbulence extent of gasification agents. It should be noted that, however, this mass transfer resistance, from the bulk gas flow to the surface of solid, varies little with the flow rate of gasification agents in the channel of UCG because they are perpendicular to each other [20] (pp. 1835–1836). Huang et al. [21] showed the vertical velocity to the surface is mainly affected by the permeability and fracture of solid, rather than the air flow rate in the axle direction.

Since it is hard to reduce diffusion resistance in ash layer in UCG by manipulating the operating conditions only a few studies addressed the diffusion behavior of gasification agents in ash layer, and most of them assumed a constant diffusion coefficient in the ash layer. However, many coal gasification and combustion studies, other than those of UCG, showed obvious changes in ash structure during the course of gasification, so do the mass transfer coefficients. For instance, Barea et al. [22] suggested the effective diffusion coefficients of CO₂ depends on temperature and porosity of char, and obvious mass transfer resistance was found in char bed as thin as several millimeters in a TGA study. Yan [23] studied combustion of 10 coals and showed that the diffusion coefficient is proportional to effective porosity in ash layers. Liu [24] studied the anisotropy of the ash layer of oil shale, showed that the diffusion coefficients increased with increasing ash layer thickness, but the reaction turns to internal diffusion control under an ash layer of several millimeters.

Due to the importance of mass transfer in ash layer in UCG and little information can be found in the literature on the subject, this work studies the mass transfer behavior of O₂ with increasing thickness of ash layer at various temperatures and O₂ concentrations using a specially designed one-dimensional gasification setup in a TGA.

2. Materials and Methods

2.1. Theoretical Section

In principle, as shown in Figure 1, the mass transfer of O₂ during the gasification of char with an ash layer includes the following steps: (a) diffusion of O₂ with a concentration of C_f in the bulk gas to the external surface of the ash layer, (b) diffusion of O₂ with a concentration of C_{S1} at the surface of ash layer to the char interface, and (c) reaction of O₂ with a concentration of C_{S2} at the char interface with char following the first order reaction [25] respecting to O₂ to produce CO then to CO₂ as shown in our previous study [26]. Under the quasi-steady state, the flux of O₂ (N_{O_2}) from the bulk gas to the external surface of ash layer is equal to the flux of O₂ diffusing through the ash layer, as well as to the reaction of O₂ at the char interface. These steps can be expressed by Equation (1), where K_c is the mass transfer coefficient of convection, L is the thickness of ash layer, D_e is the effective diffusivity in the ash layer, K is the rate constant of C-O₂ reaction, while C_f , C_{S1} and C_{S2} are O₂ concentration in the gas bulk, at the external surface of ash layer, and at the char surface, respectively:

$$N_{O_2} = K_c(C_f - C_{S1}) = \frac{D_e}{L}(C_{S1} - C_{S2}) = KC_{S2} \quad (1)$$

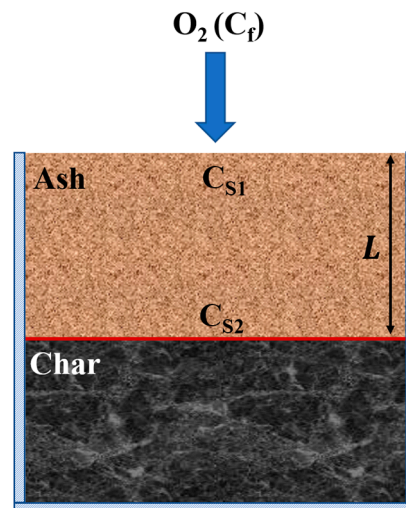


Figure 1. Schematic representation of a char sample with one-dimensional ash layer formation.

N_{O_2} can also be expressed by Equation (2) in terms of mass transfer resistance of these steps or by Equation (3) in terms of carbon consumption rate at the char surface. In these equations M_C is molecular mass of carbon (char), dn_c/dt is carbon consumption rate in mole/min, dm/dt is carbon consumption rate in g/min, and DTG is mass loss rate of sample in g/min measured by TGA. Based on these equations D_e can be expressed by Equation (4).

$$N_{O_2} = \frac{C_f}{\frac{1}{K_c} + \frac{L}{D_e} + \frac{1}{K}} \quad (2)$$

$$N_{O_2} = -\frac{dn_C}{dt} = -\left(\frac{1}{M_C} \frac{dm}{dt}\right) = -\frac{DTG}{M_C} \quad (3)$$

$$D_e = \frac{L}{-\frac{M_C C_f}{DTG} - \left(\frac{1}{K_c} + \frac{1}{K}\right)} \quad (4)$$

Since the ash layer thickness L at a given gasification time is not easy to be determined accurately by the sample's appearance it is estimated from the amount of carbon gasified by Equation (5) based on the following assumptions: (a) The cylindrical char samples consist of C and ash only, and they are distributed uniformly; (b) The ash remained in the gasification maintains the same cylindrical shape as the char sample; and (c) There is no C in the ash layer. In Equation (5), L_f is the final ash layer thickness in an experiment, Δm and Δm_f are the mass losses at the given time and the end of the experiment, respectively.

$$L = \frac{\Delta m}{\Delta m_f} \times L_f \quad (5)$$

The rate constant of C-O₂ reaction (K) can be expressed by Equation (6), where A , E_a , R and T are the pre-exponential factor, the apparent activation energy, the gas constant, and temperature, respectively.

$$K = AT^n e^{-E_a/RT} \quad (6)$$

The convective mass-transfer coefficient (K_c) can be estimated by the Sherwood number (Sh) that is the ratio of convective mass transfer and diffusion mass transfer as shown in Equation (7), where L' is the feature size of char sample, D_{O_2} is the molecular diffusivity of oxygen in the bulk gas.

$$Sh = \frac{K_c L'}{D_{O_2}} \quad (7)$$

When the fluid flows through a single particle as in this paper, the Sherwood number can be approximated by Equation (8) according to Bews et al. [27], where Re is the Reynolds number, Sc is the Schmidt number, d is the inner diameter of TGA tube, u is the flow velocity, ν is the kinematic viscosity of gas flow.

$$Sh = 2.0 + 0.69Sc^{1/3}Re^{1/2} = 2.0 + 0.69\left(\frac{\nu}{D_{O_2}}\right)^{1/3}\left(\frac{ud}{\nu}\right)^{1/2} \quad (8)$$

The combination of Equations (7) and (8) yields Equation (9) for K_c .

$$K_c = \frac{D_{O_2}}{L'}(2.0 + 0.69\left(\frac{\nu}{D_{O_2}}\right)^{1/3}\left(\frac{ud}{\nu}\right)^{1/2}) \quad (9)$$

2.2. Experimental Section

A Chinese low volatile bituminous coal, Luxian coal, is used in the study. After pyrolysis at 1173 K in N_2 for 3 h, a char with 37 wt. % ash was obtained. The char was crushed and sieved to 60–100 mesh size and then pressed to cylindrical form of 10 mm in diameter and 9 mm in length. The porosity of cylindrical char sample is 0.37, similar to that of the char prior to crushing, 0.35. The purpose of crushing and pelletizing the char is to minimize the macroscopic anisotropy of char structure [24]. In addition, the diameter range of crashed char powder, 0.15–0.25 mm, is much larger than the mean free path of O_2 and the size of the large pores (around 0.0001 mm).

The cylindrical char sample is enclosed in a size-compatible cylindrical TGA crucible with an inner diameter of 10 mm and a depth of 9 mm as shown in Figure 2. Since only the top of char sample is in contact with the gasification reagent, the gasification proceeds along the axial direction with a constant gasification area and the ash layer remained in the gasification maintains the cylindrical shape as the char, similar to that described by the shrinking-core model [28]. After been heated to a gasification temperature in Ar at a rate of 20 K/min, the char sample was exposed to a flow of 10% O_2 in balance Ar at a rate of 100 mL/min, which replaced 99% Ar in the TGA in 5 min. After a given gasification time, the gas flow was switched to Ar and the char sample was cool down to room temperature. Re at 1273 K is about 5, the same magnitude as that reported on the coal surface in an underground study [21].



Figure 2. The appearance of char sample before and after gasification at 1273 K for 99 min.

3. Results and Discussion

Figure 3 shows the cross-section view of samples gasified at 1273 K for about 19 and 99 min with mass losses of 90 and 338 mg, respectively. Clearly the gasification front moves along the axial direction of the cylindrical char as expected by the one-dimensional shrinking-core model and the ash remained adheres to the char surface to form a layer of similar thickness. The ash shrinks slightly as evidenced in the radial direction and small amounts of char at the lateral surface closing to the reacting front

gasify due to diffusion of O_2 into the gap between the crucible wall and the sample. Based on the ash layer of 4.0 mm thick in the axis at a mass loss of 338 mg an ash layer of 1.07 mm thick is determined by Equation (5) for a mass loss of 90 mg, which is very close to the observed ash layer thickness of 1.02 mm, indicating sufficient accuracy of Equation (5) in estimating the ash layer thickness.



Figure 3. The cross-section view of a sample gasified at 1273 K to different mass losses.

Figure 4 shows the TG and DTG curves of char gasification at 1273 K which yield the samples in Figure 3. The maximum gasification rate (DTG) appears at the beginning, about 5.42 mg/min, due to the absence of an ash layer. As the gasification proceeds, the DTG decreases continuously to about 2.47 mg/min at 99 min, indicating an increase in diffusion resistance of O_2 with an increase in ash layer thickness. This behavior, however, may also include changes in the effective diffusion coefficient D_e .

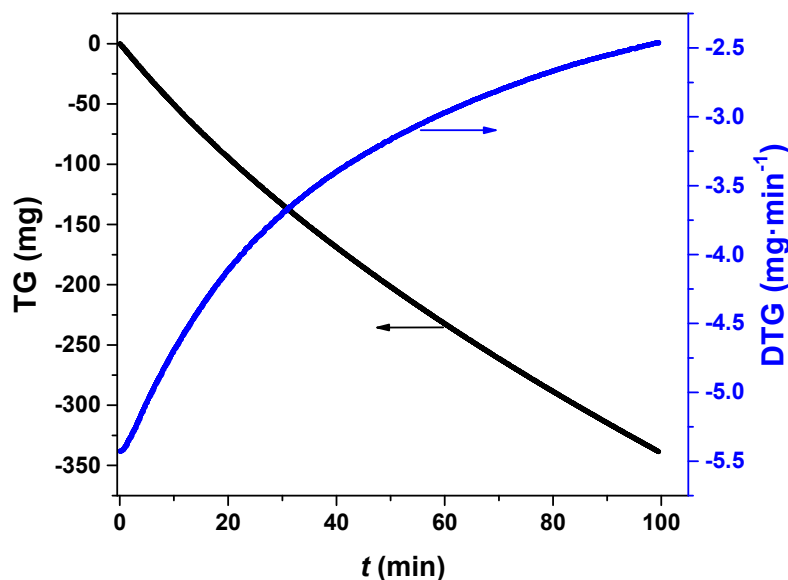


Figure 4. TG and DTG curves during gasification at 1273 K.

3.1. Estimation of Effective Diffusion Coefficient

Since the gasification temperature in Figures 3 and 4 is higher than 1173 K, the boundary of oxidation zone in the “three zones theory” [29], higher than which the resistance of C- O_2 reaction is negligible compared with that of interparticle diffusion [30], Equation (4) can be simplified to Equation (10).

$$D_e = \frac{L}{-\frac{M_c C_f}{DTG} - \frac{1}{K_c}} \quad (10)$$

Figure 5 shows D_e determined by Equation (10). As expected D_e increases with an increase in temperature, $1.51 \times 10^{-4} \text{ m}^2/\text{s}$ at 1173 K while $2.82 \times 10^{-4} \text{ m}^2/\text{s}$ at 1373 K both at the mass loss of 250 mg, corresponding to an ash layer thickness of 3 mm. The range of D_e is the same as that determined in our previous study [26] in coal gasification (around $1 \times 10^{-4} \text{ m}^2/\text{s}$) and that reported by Chen et al. [31] for combustion of coal particles of 16 mm in diameter with 53% ash ($1.5 \times 10^{-4} \text{ m}^2/\text{s}$ at 1145 K). Figure 5 also shows that D_e increases with increasing time, indicating increasing pore size or fractures in the ash layer over time. This behavior is similar to that reported by Sotirchos [32], who studied combustion of a char with 25% ash and showed increasing macropore volume over time for ash layers of millimeter thick, and increasing D_e over time in a range around $1 \times 10^{-4} \text{ m}^2/\text{s}$ at 1173 K. Clearly, the compressed cylindrical char sample prepared in this work can be used to study D_e of char particles.

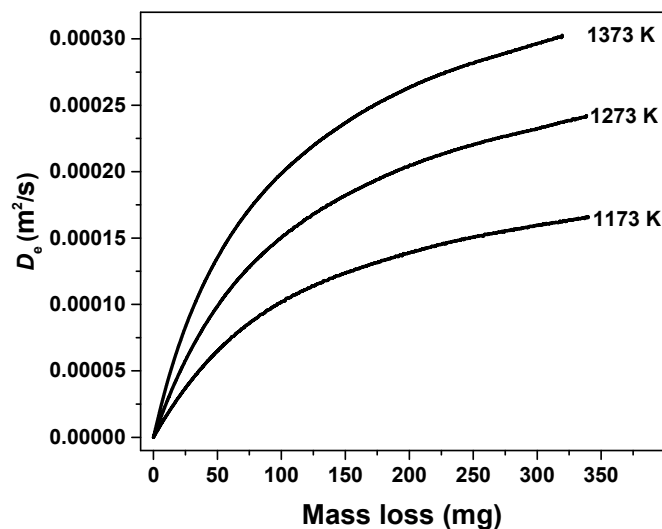


Figure 5. Diffusion coefficient at different temperatures in gasification.

It is noted that in addition to porosity, pore size distribution in the ash layer may also influence mass transfer rate of O_2 . To explore this effect ash layers formed on cylindrical char samples during gasification at 1273 K for different time, as shown in Figure 6, were sampled at every 2 mm thick and subjected to mercury intrusion porosimetry analysis. The ash samples listed in Table 1 are these formed initially, 0–2 mm in Figure 6a (Sample 1); 0–2 mm in Figure 6b (Sample 2) that exposed to 1273 K longer than that of Sample 1; 2–4 mm in Figure 6b (Sample 3); and that exposed to 1273 K for a time much longer than other samples (Sample 4) in addition. The t in the table is the residence time the ash sample exposed to 1273 K. It seems that the porosity of these samples is similar, around 0.7, but the median pore diameter of these samples increases with an increase in gasification time, from about 1400 nm in 20–30 min to 1700 nm in 175 min. Since these median pore diameters are less than 5 times the mean free path of O_2 at 1273 K (about 381 nm), in which the collision between gas molecule and the pore wall cannot be ignored, so the increasing D_e in gasification in Figure 5 can be attributed to increasing pore diameter in the ash layers during the gasification.

Table 1. Median pore diameter of ash samples from gasification at 1273 K for different time.

Parameter	Sample 1	Sample 3	Sample 2	Sample 4
t (min)	20	30	65	175
Porosity	0.68	0.69	0.70	0.70
diameter (nm)	1397	1401	1601	1710

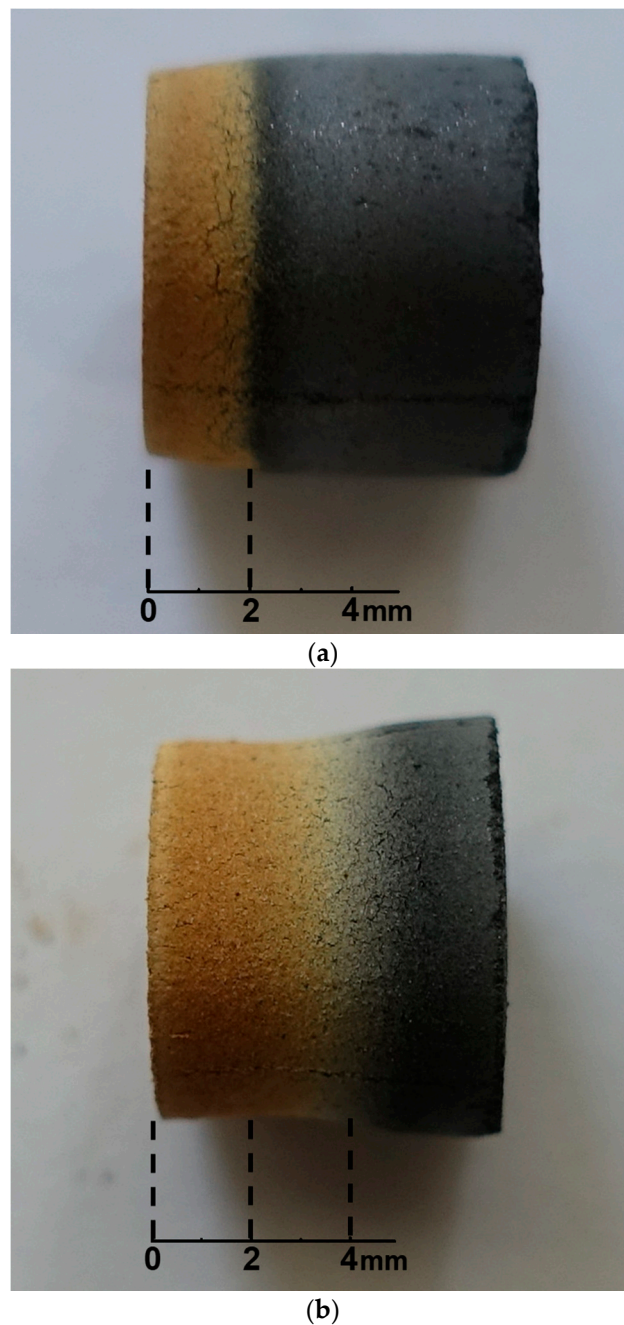


Figure 6. Samples subjected to gasification at 1273 K for different time: (a) with an ash layer of 2 mm; (b) with an ash layer of 4 mm.

3.2. Internal Diffusion Resistance

For a one-dimensional gas-solid reaction, the traditional shrinking-core model suggests a linear relationship between reaction time (t) and square of ash thickness (L) if internal diffusion is the rate limiting step and effective diffusivity D_e is constant [33]. The plot in Figure 7 shows that the $L-t^{0.5}$ relation of this work is close to a linear relation at ash layer thickness of greater than 2 mm. This however does not necessarily indicate that the gasification is under internal diffusion control because the D_e in the ash layer varies with ash layer thickness as indicated in Figure 5.

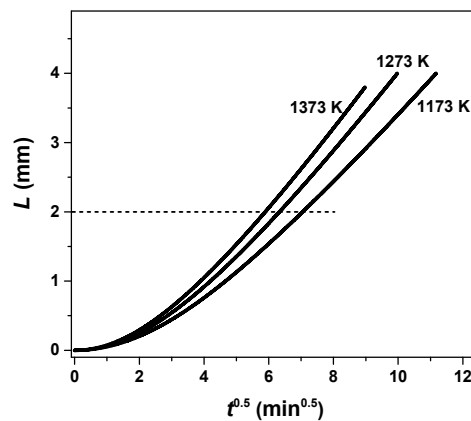


Figure 7. Relation between $t^{0.5}$ and thickness of ash layer L .

To understand the role of O_2 diffusion in ash layer the internal diffusion resistance (L/D_e) at the ash layer thickness of 1, 2 and 3 mm is compared with the reaction resistance at the char surface ($1/K$) and the convection resistance in the bulk gas ($1/K_c$) in Table 2. The $1/K$ and $1/K_c$ are determined by Equations (6) and (9) based on the experimental data of this work and those in the literature [34]. It can be seen that the reaction resistance ($1/K$) is much smaller than the diffusion resistances of $1/K_c$ and L/D_e under the conditions used, indicating that the overall gasification rate is always under mass transfer control. The L/D_e increases with an increase in ash layer thickness although D_e also increases with an increase in ash layer thickness as shown in Figure 5, suggesting that the diffusion resistance of O_2 in the ash layer is more affected by L than by D_e .

Table 2. Resistance of reaction and mass transfer in gas film and ash layer (s/m).

Resistance	1173 K	1273 K	1373 K
$1/K$	0.3	0.07	0.02
$1/K_c$	6.4	5.6	5.0
L/D_e ($L = 1$ mm)	10.8	7.3	5.5
L/D_e ($L = 2$ mm)	15.4	10.5	8.1
L/D_e ($L = 3$ mm)	19.8	13.5	10.6

The contribution of L/D_e to overall mass transfer resistance (η) can be determined with sufficient accuracy by Equation (11), ignoring the contribution of $1/K$, and shown in Figure 8. Clearly, η increases nonlinearly with an increase in ash layer thickness while decreases almost linearly with an increase in temperature, and the O_2 diffusion in ash layer plays a dominant role especially when the ash layer thickness is greater than 1 mm. For instance, at 1273 K, $1/K_c$ is 5.6 s/m while η is around 70% at an ash thickness of 3 mm, corresponding to a mass loss about 250 mg. This η indicates that the diffusion resistance in ash layer is more than twice as much as the external diffusion resistance. This increase in diffusion resistance in the ash layer leads to a decrease in O_2 diffusion rate and a decrease in overall gasification rate, by about 50% from the initial value as indicated in Figure 4. This behavior is similar to that reported by Perkins et al. [35] in which a 20% reduction in gasification rate was observed at an ash layer of 1 mm thick in a meter-scale UCG simulation study.

$$\eta = \frac{L/D_e}{\frac{L}{D_e} + \frac{1}{K_c}} \times 100\% \quad (11)$$

The temperature effect on η in Figure 8 shows that the diffusion resistance in ash layer is more important at a lower temperature than that at a higher temperature. For instance, at an ash layer thickness of 3 mm, the η is about 75.5% at 1173 K but 70.7% and 68.0% at 1273 and 1373 K, respectively.

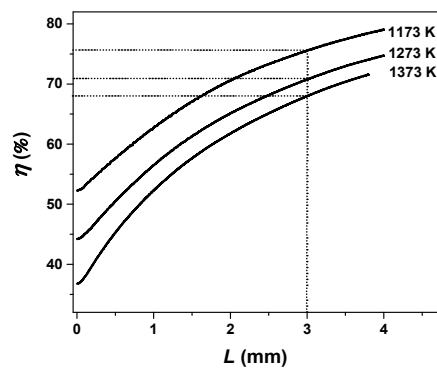


Figure 8. The contribution of L/D_e to overall mass transfer resistance (η) at different ash layer thickness.

3.3. The Influence of Gas Concentration

In UCG, O_2 concentration decreases from the injection well to the production well due to its consumption in gasification. A higher O_2 concentration leads to a higher gasification rate and perhaps also to a change in D_e due to local melting of ash caused by the heat of reaction between O_2 and CO in the ash layer as indicated in our earlier study [26]. It can be seen in Figure 9 that at 1273 K the gasification rate increases with an increase in O_2 concentration, the time needed for gasifying 300 mg char is 115 min under 7.5% O_2 but 72 min under 12% O_2 . It can also be seen in Figure 10 that D_e determined by Equation (10) varies little with O_2 concentration at the temperatures used, indicating little ash melting under these conditions, agreeing with our earlier study that the apparent ash melting of this particular coal is at 1573 K [26]. The data in Figure 10 suggest that O_2 concentration plays a minor role while temperature and ash layer thickness play major roles in D_e in Equation (10).

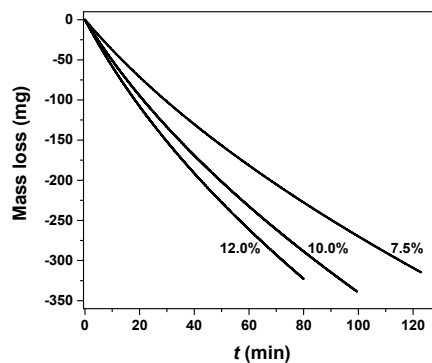


Figure 9. Gasification at 1273 K under different O_2 concentrations.

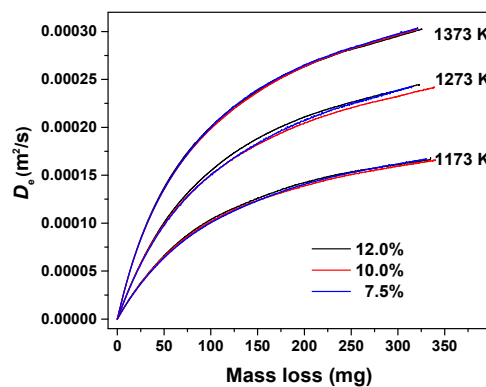


Figure 10. Effective diffusion coefficient in ash layer under different temperatures and O_2 concentrations.

3.4. Effective Diffusion Coefficient with Temperature and Ash Layer Thickness

Since it is not easy to obtain flow parameters in UCG and therefore to estimate $1/K_c$, and the $1/K_c$ is smaller than L/D_e when ash layer is thick, Equation (10) can be simplified to Equation (12) by omitting $1/K_c$ with accuracy θ defined by Equation (13). It can be seen in Figure 11 that θ increases with an increase in ash layer thickness and is higher than 50% when ash layer thickness is higher than 1 mm, especially at low temperatures. For instance, at 1273 K, θ is 44% initially but becomes 76% at an ash layer thickness of 4 mm. Clearly in a continuous operation of UCG with a much thicker ash layer the O_2 diffusion resistance in ash layer is the dominant resistance.

$$D'_e = -\frac{L \times DTG}{M_C C_f} \quad (12)$$

$$\theta = \frac{D'_e}{D_e} \times 100\% = \frac{DTG}{DTG + \frac{M_C C_f}{K_c}} \times 100\% \quad (13)$$

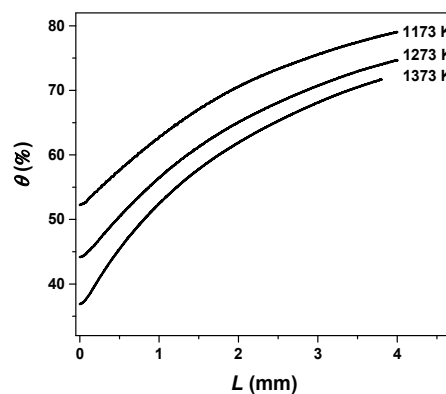


Figure 11. Accuracy of diffusion coefficient (θ) under omitting external diffusion resistance.

Since L/D_e dominates the overall mass transfer resistance in UCG it is useful to establish a relation between D_e in the ash layer and the D_{O_2} in the bulk gas. At a reaction temperature this relation however involves correlations in two regions separated by the pore size that is 10 times the mean free path of O_2 , 10λ , i.e., free diffusion in pores (and fractures) of larger than 10λ in size with the coefficient approximately D_{O_2} and restrictive diffusion in pores of smaller than 10λ in size with a coefficient D_1 , which is smaller than D_{O_2} . Previous study [36] suggested that D_1 is proportional to the porosity as shown in Equation (14), where ε_1 is porosity of the pores with diameters less than 10λ and τ is tortuosity of pores generally within 2 to 6 [37].

$$D_1 = \frac{\varepsilon_1}{\tau} \times D_{O_2} \quad (14)$$

$$D_e = (0.7 - \varepsilon_1)D_{O_2} + \varepsilon_1 D_1 \quad (15)$$

$$D_e = D_{O_2} \left(0.7 - \varepsilon_1 + \frac{\varepsilon_1^2}{\tau} \right) \quad (16)$$

As shown in Table 1 the total porosity of ash layer is approximately 0.7, hence the fraction of pores with diameter larger than 10λ is $0.7 - \varepsilon_1$ which is also the porosity of any cross section in the ash layer [38]. The effective diffusion coefficient D_e therefore can be expressed by Equation (15), and the relation between D_e and D_{O_2} can be expressed as Equation (16).

If the pores in the ash layer coalesce in continuous high temperature UCG operation ε_1 can be described by Equation (17) according to the format of relationship between porosity and time in porous ceramics at high temperature [39] (p. 380), where t is time while B and c are parameters obtained by

fitting experimental data. Then Equation (16) can be rewritten as Equation (18) and then Equation (19) because time t is proportionate linearly with the square of ash layer thickness as discussed earlier.

$$\varepsilon_1 = Be^{-ct} \quad (17)$$

$$D_e = D_{O_2}(0.7 - Be^{-ct} + \frac{B^2}{\tau} \times (e^{-ct})^2) \quad (18)$$

$$D_e = D_{O_2}(0.7 - Be^{-cdL^2} + \frac{B^2}{\tau}(e^{-cdL^2})^2) \quad (19)$$

Since the higher-order term in Equation (20), $\frac{B^2}{\tau}(e^{-cdL^2})^2$, is relatively small at a higher ash layer thickness and can be omitted, and D_{O_2} is proportional to $T^{1.75}$ according to the formula proposed by Fuller Schettler Giddings [38] Equation (19) can be rewritten as Equation (20) with F as the product of c and d .

$$D_e = 1.78 \times 10^{-5} \left(\frac{T}{273}\right)^{1.75} (0.7 - Be^{-FL^2}) \quad (20)$$

Table 3 shows the parameters B and F determined by fitting Equation (20) with the data at 1173, 1273 and 1373 K using the least squares method. It can be found that B changes little with a change in temperature indicating that B is determined by the physical properties of ash layer, while F varies relatively strongly with temperature.

Table 3. Parameters of Equation (20).

Parameter	1173 K	1273 K	1373 K
B	0.530	0.548	0.556
F	114,914	210,240	279,638

Figure 12 shows D_e determined by Equation (20) and that observed in the experiments (dots) under different temperatures and ash layer thickness. Clearly the D_e determined from Equation (20) fits the experimental data well with small residual sum of square, approximately $7.1 \times 10^{-11} \text{ m}^4/\text{s}^2$ at 1273 K and ash layer thickness of 2.5–3.5 mm, for example.

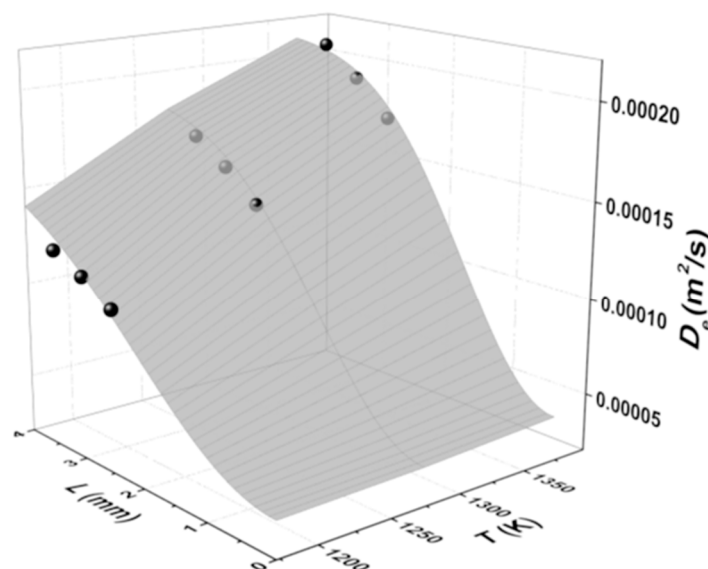


Figure 12. Diffusion coefficient in ash layer under different temperature and ash layer thickness.

Figure 13 shows η , the proportion of internal diffusion resistance in overall mass transfer resistance defined earlier by Equation (11), under different temperatures and ash layer thickness. The contours of η of 70, 75 and 80% show that the internal diffusion resistance plays a major role in overall mass transfer resistance, more than 75% when the ash layer is thicker than 2.5 mm at 1250–1300 K, for example.

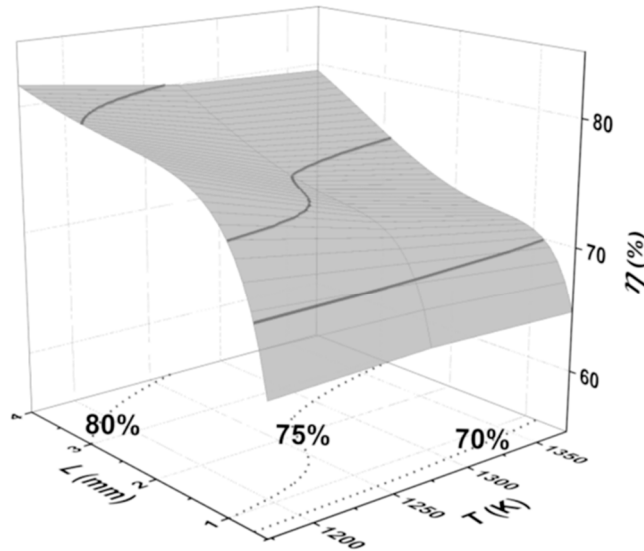


Figure 13. The contribution of L/D_e to overall mass transfer resistance (η) under different temperatures and ash layer thickness.

The increase in η with increasing ash layer thickness would reduce the O_2 flux through ash layer leading to reduced gasification rate and low char conversion, as well as a shift of gasification zone toward the downstream in a UCG operation. This agrees with that reported in the field test [40], where 30% char was not converted even though spalling of coal and ash were observed.

4. Conclusions

This paper studies mass transfer of oxygen in ash layer of UCG using cylindrical char samples in a TGA. It is found that an ash layer is formed and remained on the surface of char, which reduces the rate of carbon conversion significantly in gasification. The effective internal diffusion coefficient of O_2 (D_e) is estimated based on the ash layer thickness observed and estimated from carbon conversion. The mean pore diameter of ash layer increases with an increase in ash layer thickness, so does the D_e . The mass transfer resistance of O_2 in the ash layer (L/D_e) also increases with an increase in ash layer thickness, which is the dominant resistance when the ash layer is a few millimeters thick.

Acknowledgments: The work is financially supported by the National Key Research and Development Program of China (2016YFB0600300).

Author Contributions: Zhenyu Liu and Qingya Liu designed research; Xi Lin performed the experiment; Xi Lin and Qingya Liu analyzed the data; Xi Lin and Zhenyu Liu wrote the paper.

Conflicts of Interest: The authors declare no conflict of interest.

References

1. Najafi, M.; Jalali, S.M.E.; KhaloKakaie, R. Thermal–mechanical–numerical analysis of stress distribution in the vicinity of underground coal gasification (UCG) panels. *Int. J. Coal Geol.* **2014**, *134–135*, 1–16. [[CrossRef](#)]
2. Otto, C.; Kempka, T. Prediction of steam jacket dynamics and water balances in underground coal gasification. *Energies* **2017**, *10*, 739. [[CrossRef](#)]
3. Shafirovich, E.; Varma, A. Underground coal gasification: a brief review of current status. *Ind. Eng. Chem. Res.* **2009**, *48*, 7865–7875. [[CrossRef](#)]

4. Urych, B. Determination of kinetic parameters of coal pyrolysis to simulate the process of underground coal gasification (UCG). *J. Sustain. Min.* **2014**, *13*, 3–9. [[CrossRef](#)]
5. Prabu, V.; Jayanti, S. Simulation of cavity formation in underground coal gasification using bore hole combustion experiments. *Energy* **2011**, *36*, 5854–5864. [[CrossRef](#)]
6. Konstantinou, E.; Marsh, R. Experimental study on the impact of reactant gas pressure in the conversion of coal char to combustible gas products in the context of underground coal gasification. *Fuel* **2015**, *159*, 508–518. [[CrossRef](#)]
7. Hamanaka, A.; Su, F.; Itakura, K.; Takahashi, K.; Kodama, J.; Deguchi, G. Effect of injection flow rate on product gas quality in underground coal gasification (UCG) based on laboratory scale experiment: development of Co-Axial UCG system. *Energies* **2017**, *10*, 238. [[CrossRef](#)]
8. Ollero, P.; Serrera, A.; Arjona, R.; Alcantarilla, S. Diffusional effects in TGA gasification experiments for kinetic determination. *Fuel* **2002**, *81*, 1989–2000. [[CrossRef](#)]
9. Sadhukhan, A.K.; Gupta, P.; Saha, R.K. Modelling of combustion characteristics of high ash coal char particles at high pressure: shrinking reactive core model. *Fuel* **2010**, *89*, 162–169. [[CrossRef](#)]
10. Park, K.Y.; Edgar, T.F. Modeling of early cavity growth for underground coal gasification. *Ind. Eng. Chem. Res.* **1987**, *26*, 237–246. [[CrossRef](#)]
11. Perkins, G.; Sahajwalla, V. Modelling of heat and mass transport phenomena and chemical reaction in underground coal gasification. *Chem. Eng. Res. Des.* **2007**, *85*, 329–343. [[CrossRef](#)]
12. Su, F.; Nakanowataru, T.; Itakura, K.; Ohga, K.; Deguchi, G. Evaluation of structural changes in the coal specimen heating process and UCG model experiments for developing efficient UCG Systems. *Energies* **2013**, *6*, 2386–2406. [[CrossRef](#)]
13. Prabu, V.; Jayanti, S. Heat-affected zone analysis of high ash coals during ex-situ experimental simulation of underground coal gasification. *Fuel* **2014**, *123*, 167–174. [[CrossRef](#)]
14. Wang, Z.; Liang, J.; Shi, L.; Xi, J.; Li, S.; Cui, Y. Expansion of three reaction zones during underground coal gasification with free and percolation channels. *Fuel* **2017**, *190*, 435–443. [[CrossRef](#)]
15. Daggupati, S.; Mandapati, R.N.; Mahajani, S.M.; Ganesh, A.; Mathur, D.K.; Sharma, R.K.; Aghalayam, P. Laboratory studies on combustion cavity growth in lignite coal blocks in the context of underground coal gasification. *Energy* **2010**, *35*, 2374–2386. [[CrossRef](#)]
16. Cena, R.J.; Britten, J.A.; Thorsness, C.B. Excavation of the partial CRIP underground coal gasification test site. In Proceedings of the 13th Annual Underground Coal Gasification Symposium, Laramie, WY, USA, 24–30 August 1987.
17. Yang, L.H. Three-Dimensional non-linear numerical analysis on the oxygen concentration field in underground coal gasification. *Fuel Process. Technol.* **2004**, *85*, 1605–1622. [[CrossRef](#)]
18. Eftekhari, A.A.; Wolf, K.H.; Rogut, J.; Bruining, H. Mathematical modeling of alternating injection of oxygen and steam in underground coal gasification. *Int. J. Coal Geol.* **2015**, *150*, 154–165. [[CrossRef](#)]
19. Kuyper, R.A.; Meer, T.H.V.D.; Hoogendoorn, C.J. Turbulent natural convection flow due to combined buoyancy forces during underground coal gasification of thin seams. *Chem. Eng. Sci.* **1994**, *49*, 851–861. [[CrossRef](#)]
20. Elliott, M.A. *Chemistry of Coal Utilization*; John Wiley and Sons: New York, NY, USA, 1981; pp. 1835–1836.
21. Huang, J.; Bruining, J.; Wolf, K.-H.A.A. Modeling of gas flow and temperature fields in underground coal fires. *Fire Saf. J.* **2001**, *36*, 477–489. [[CrossRef](#)]
22. Barea, A.G.; Ollero, P.; Arjona, R. Reaction-diffusion model of TGA gasification experiments for estimating diffusional effects. *Fuel* **2005**, *84*, 1695–1704. [[CrossRef](#)]
23. Yan, J.; Ni, M.; Zhao, H.; Cen, K. Gas diffusion through the ash layer of coal particle during the combustion process. *Int. J. Thermophys.* **1994**, *15*, 341–344. [[CrossRef](#)]
24. Liu, J.G.; Yan, J.W.; Han, X.X.; Jiang, X.M. Study on the anisotropy of mass transfer for oxygen in the ash layer of shale char particles. *Energy Fuels* **2010**, *24*, 3488–3497. [[CrossRef](#)]
25. Hwang, M.; Song, E.; Song, J. One-dimensional modeling of an entrained coal gasification process using kinetic parameters. *Energies* **2016**, *9*, 99. [[CrossRef](#)]
26. Lin, X.; Liu, Q.; Liu, Z.; Guo, X.; Wang, R.; Shi, L. The role of ash layer in syngas combustion in underground coal gasification. *Fuel Process. Technol.* **2016**, *143*, 169–175. [[CrossRef](#)]
27. Bews, I.M.; Hayhurst, A.N.; Richardson, S.M.; Taylor, S.G. The order, Arrhenius parameters, and mechanism of the reaction between gaseous oxygen and solid carbon. *Combust. Flame* **2001**, *124*, 231–245. [[CrossRef](#)]

28. Khan, M.M.; Mmbaga, J.P.; Shirazi, A.S.; Trivedi, J.; Liu, Q.; Gupta, R. Modelling underground coal gasification—A review. *Energies* **2015**, *8*, 12603–12668. [[CrossRef](#)]
29. Yang, L.H.; Zhang, X.; Liu, S.Q.; Yu, L.; Zhang, W.L. Field test of large-scale hydrogen manufacturing from underground coal gasification (UCG). *Int. J. Hydrogen Energy* **2008**, *33*, 1275–1285. [[CrossRef](#)]
30. Su, J.L.; Perlmutter, D.D. Effect of Pore Structure on Char Oxidation Kinetics. *AIChE J.* **1985**, *31*, 973–981. [[CrossRef](#)]
31. Chen, C.; Kojima, T. Single char particle combustion at moderate temperature: effects of ash. *Fuel Process. Technol.* **1996**, *47*, 215–232. [[CrossRef](#)]
32. Sotirchos, S.V.; Amundson, N.R. Dynamic behavior of a porous char particle burning in an oxygen-containing environment. *AIChE J.* **1984**, *30*, 537–549. [[CrossRef](#)]
33. Wen, C.Y. Non-Catalytic Heterogeneous Solid-Fluid Reaction Models. *Ind. Eng. Chem.* **1968**, *60*, 34–54. [[CrossRef](#)]
34. Perkins, G. Mathematical Modelling of Underground Coal Gasification. Ph.D. Thesis, The University of New South Wales, Sydney, Australia, 2005.
35. Perkins, G.; Sahajwalla, V. A numerical study of the effects of operating conditions and coal properties on cavity growth in underground coal gasification. *Energy Fuels* **2006**, *20*, 596–608. [[CrossRef](#)]
36. Sadhukhan, A.K.; Gupta, P.; Saha, R.K. Analysis of the dynamics of coal char combustion with ignition and extinction phenomena: shrinking core model. *Int. J. Chem. Kinet.* **2008**, *40*, 569–582. [[CrossRef](#)]
37. Kelebopile, L.; Sun, R.; Wang, H.; Zhang, X.; Wu, S.H. Pore development and combustion behavior of gasified semi-char in a drop tube furnace. *Fuel Process. Technol.* **2013**, *111*, 42–54. [[CrossRef](#)]
38. Parlange, J.Y. Reviewed Work: Dynamics of Fluids in Porous Media by J. BEAR. *Am. Sci.* **1973**, *6*, 758–759.
39. Kingery, W.D. *Introduction to Ceramics*, 1st ed.; Wiley: New York, NY, USA, 1960; p. 380, ISBN 0471478601.
40. Hill, R.W.; Hill, C.B. *Summary Report on Large Block Experiments in Underground Coal Gasification, Tono Basin, Washington: Volume 1. Experimental Description and Data Analysis*; Report No. UCRL-53305; Lawrence Livermore National Laboratory, University of California: Berkeley, CA, USA, 9 July 1982.



© 2018 by the authors. Licensee MDPI, Basel, Switzerland. This article is an open access article distributed under the terms and conditions of the Creative Commons Attribution (CC BY) license (<http://creativecommons.org/licenses/by/4.0/>).